The effect of spatial confinement on magnetism: films, stripes and dots of Fe on Cu(111)

2003 J. Phys.: Condens. Matter 15 R1

(http://iopscience.iop.org/0953-8984/15/2/201)

INSTITUTE OF PHYSICS PUBLISHING JOURNAL OF PHYSICS: CONDENSED MATTER

J. Phys.: Condens. Matter **15** (2003) R1–R30 PII: S0953-8984(03)33359-4

TOPICAL REVIEW

The effect of spatial confinement on magnetism: films, stripes and dots of Fe on Cu(111)

J Shen[1], **J P Pierce**[1,2], **E W Plummer**[1,2] **and J Kirschner**[3]

[1] Solid State Division, Oak Ridge National Laboratory, Oak Ridge, TN 37831, USA
[2] Department of Physics, University of Tennessee, Knoxville, TN 37996, USA
[3] Max-Planck-Institut f. Mikrostrukturphysik, Weinberg 2, D-06120 Halle/Saale, Germany

Received 14 August 2002
Published 20 December 2002
Online at stacks.iop.org/JPhysCM/15/R1

Abstract

In this article, we review recent progress in the exploration of the complex magnetic phases of the fcc Fe/Cu(111) system. In particular, we emphasize the magnetic properties realized by the synthesis of novel nanostructures of Fe on Cu(111). These include monolayer films, one-dimensional stripe arrays and nanodot arrays. The effects of spatial confinement, together with strong spin–lattice correlations, result in dramatically different magnetic behaviour for the various manifestations of the Fe/Cu(111) system. Multi-scale theoretical calculations have been used to provide an understanding of the magnetic behaviour in each case.

(Some figures in this article are in colour only in the electronic version)

Contents

0953-8984/03/020001+30$30.00

1. Introduction

In the last decade, basic science has had a remarkable impact on practical devices in the area of magnetic recording. In less than ten years, the discovery of giant magnetoresistance, a phenomenon that occurs in thin film sandwiches of magnetic and non-magnetic materials, developed into a $100 billion per year market for a new generation of hard disk drives. This amazingly rapid progress resulted from basic research that gave the community both the ability to grow these artificial structures and a basic understanding of their behaviour that allowed optimal tuning of their properties. The rich physics associated with these magnetic films [1, 2]—which are nanoscale in only one spatial dimension—provides ample testament that nanophase magnetic materials are not just smaller but also different! As efforts to reduce device size have continued, it has become imperative to investigate the magnetic properties of artificial structures on smaller length scales and in reduced dimensionality, as in nanowires [3–8], dots [9–12] and pillars [13]. These advances, coupled with emerging techniques for synthesizing magnetic nanowires [8, 14, 15], nanoparticles [16] and molecular magnets [17, 18], have established the research of spatially confined magnetic materials as a new frontier both in basic science and technology.

New properties that emerge at the nanoscale have at least four origins:

(1) As the surface-to-volume ratio increases, material properties are increasingly dominated by surface and interface effects—a 5 nm cube of bcc Fe contains ∼12 000 atoms, ∼2000 of which are on the surface.
(2) Spatial confinement results in new quantum phenomena. The oscillatory exchange coupling [19], GMR [20], spin-dependent tunnelling [21] and exchange bias [22–24] manifest in magnetic multilayers are linked with one or both of these factors.
(3) A contribution that can perhaps be called ‘characteristic length effects’. The exotic effects seen in GMR spin valves, for example, would not be observed if the individual layers in the structure were thicker than the spin-diffusion length, which is the average distance that an electron will travel in a material before undergoing a scattering process that changes its spin.
(4) In many spin systems, like colossal magnetoresistance (CMR) materials [25] and magnetic semiconductors [26, 27], correlation effects are already important in the bulk spin structure, spin fluctuations and spin transport. In general, spatial confinement will significantly change these correlation effects.

Before the exotic magnetic and electronic properties of various nanostructures like ultrathin films, nanowires and nanodots can be explored, important strides must be made in controlling their synthesis. While state-of-the-art e-beam lithography may produce structures down to the nanometre scale, mass production of such structures by lithography or etching-based fabrication has proven to be exceptionally challenging [28, 29]. For this reason, in the past decade considerable effort has been devoted to investigating growth methods using self-assembly principles. Self-assembled magnetic nanowire and nanodot arrays have been achieved on various types of substrates.

In this paper we will review studies of the spatial confinement effect on magnetism in a highly interesting system, Fe on Cu(111). We pick this particular system because it provides a classic demonstration of the tremendous impact that novel synthesis techniques

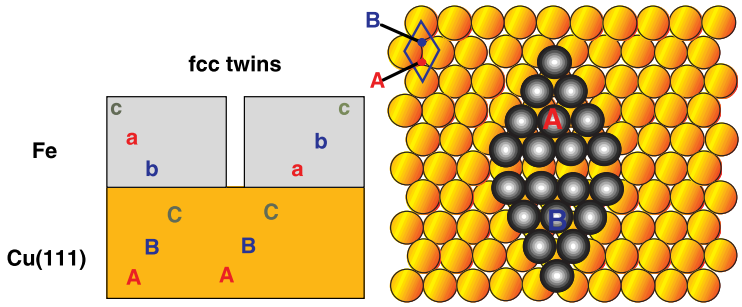

Figure 1. Schematics showing the phenomenon of twinning. The spacing between iron atoms on the Cu(111) surface is such that iron atoms in a particular island will either occupy 'A' sites only or 'B' sites only, depending on which of these two sites was settled upon by the atom that seeded the island. The image shows the fault line that forms when an A-type island tries to merge with a B-type island.

can have on the study of nanomagnetism. Ultrathin films, nanowires and nanodots of Fe have been successfully grown on the Cu(111) substrate, despite the fact that conventional growth techniques like thermal evaporation and sputter deposition do not support the growth of any of these nanostructures. The fact that these three types of nanostructures, which are spatially confined in different dimensions, can be grown on a common template allows direct observation of the effect of spatial confinement on magnetism.

Another major attraction of the Fe/Cu(111) system is that iron initially grows on this surface in the face-centred cubic structure, which is well known for its rich magnetic phases and strong spin–lattice coupling [30]. In general, a small variation of the lattice constant or lattice distortion can result in drastic changes of magnetic phases that range from low-moment ferromagnetic phase, antiferromagnetic phase, ferrimagnetic phase and high-moment ferromagnetic phases. For the very same reason, ultrathin films of fcc Fe on the Cu(100) surface have been extensively studied in the last ten years, and many exciting magnetic phase transitions [31, 32] and strong spin–lattice correlations [33, 34] have been identified. The fcc Fe/Cu(111) system, as we will soon show below, is just as exciting and its degree of complexity is just as high. Combining the results for both crystallographic orientations of fcc Fe will also lead to a better overall understanding of the material.

In order to emphasize the critical role of novel synthesis techniques in the study of low-dimensional magnetism, we organize this review as follows. In section 2 we will point out that conventional molecular beam epitaxy (thermal MBE) fails to yield any of the low-dimensional magnetic nanostructures. The structure and magnetism of the thermal MBE grown Fe/Cu(111) will be, nevertheless, discussed in that section to provide the readers with a reference point. In the following sections we discuss the growth, structure and magnetism of well ordered Fe/Cu(111) nanostructures. Ultrathin films, stripe arrays and dot assemblies of Fe on Cu(111) are described in sections 3–5, respectively. In section 6, we make a direct comparison of the magnetic properties of these manifestations of Fe on Cu(111). The final section provides a summary and an outlook on future research.

2. Thermal MBE growth of Fe on Cu(111): rough and discontinuous films

2.1. Morphology and structure

When prepared with a conventional growth technique like thermal evaporation in ultrahigh vacuum, Fe has a strong tendency to form multilayer islands on Cu(111) due, in part, to an effect called twinning. Twin structures are common features of epitaxial growth on fcc(111)

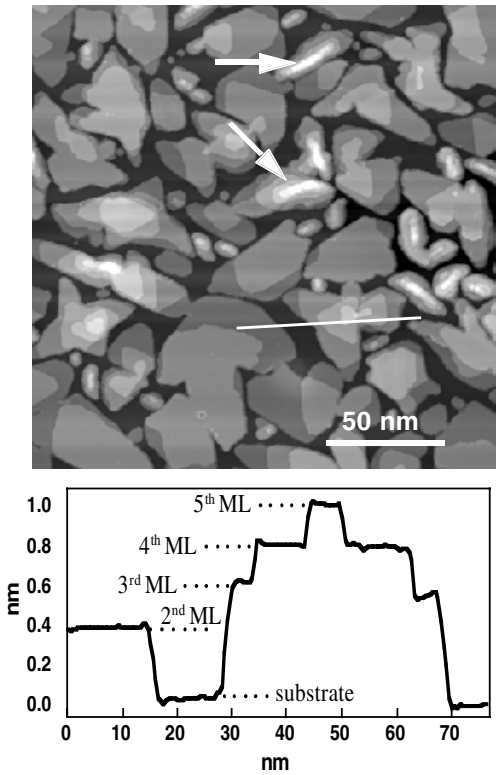

Figure 2. STM image of the rough morphology that results when two atomic layers of Fe are deposited via thermal evaporation on the Cu(111) surface at 220 K. The line scan below the image shows that this morphology is far from that of an ideal 2.0 ML film. The white arrows indicate the locations of ridge-like bcc(110) structures.

surfaces [35]. As shown in figure 1, the rhombic surface unit cell of the fcc(111) surface provides two possible sites, A and B, for adatom nucleation. Since the difference between the nucleation energies of the two sites is generally very small, an adatom has essentially no preference for one site over the other. Those that nucleate at A sites seed the growth of A-type islands, and those that nucleate at B sites lead to B-type islands. These two types of islands cannot merge to form a smooth film because a fault line, as shown in figure 1, always exists at the boundary between them.

A second feature that leads to roughness is low interlayer mass transport [36]. Because there is a high energy barrier for Fe atoms to overcome when moving from one atomic layer to the next, the thermal motion of the atoms is unable to 'heal' pits and peaks in the morphology. The consequences of fcc twinning and low interlayer mass transport can be seen in the scanning tunnelling microscope (STM) image of an Fe/Cu(111) film shown in figure 2. The film was prepared by MBE at a substrate temperature of 220 K, with the nominal Fe dosage of 2 monolayers (ML). The marked line profile shows that the typical island height is about 5 ML, and that a considerable fraction of the copper surface (darkest contrast) remains uncovered after two atomic layers of Fe are deposited.

In figure 2, another noticeable feature is the appearance of some ridge-like islands (marked by white arrows). These ridge-like structures represent the typical morphology of bcc(110) structures, which are elongated due to one-dimensional lattice matching with the fcc Cu(111)

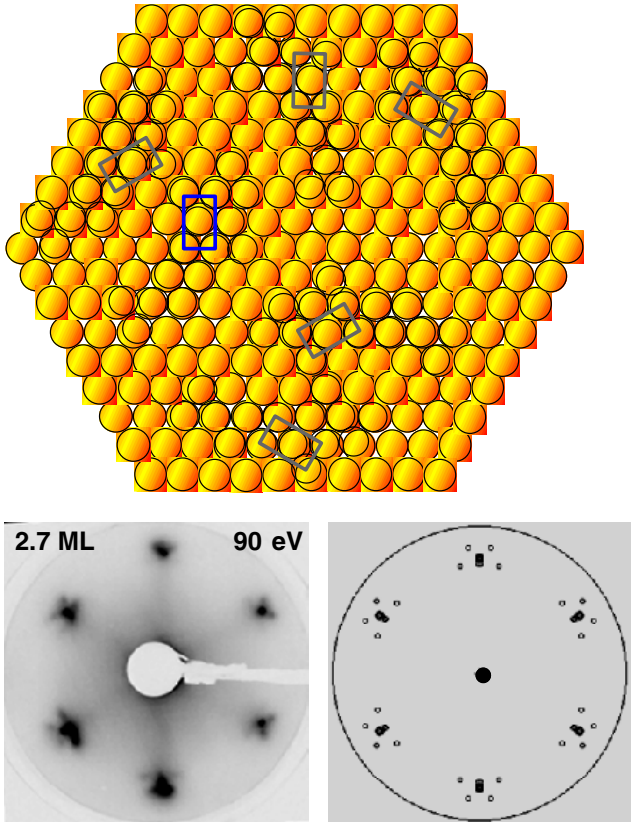

Figure 3. Ball model of Kujdimov–Sachs (KS) orientation. There are six Fe bcc(110) domains that match the Cu(111) substrate in the three ⟨110⟩ directions. At the lower left is the low-energy electron diffraction (LEED) pattern generated by a 2.7 ML thermal MBE-grown Fe on Cu(111) with KS orientation. The schematic at the lower right shows the satellite spots that form due to KS orientation.

substrate. A ball model is shown in figure 3 to demonstrate lattice matching between bcc Fe(110) and fcc Cu(111). There are, in total, six possible domain configurations (Kurdjumov–Sachs or KS orientation) along the three ⟨011⟩ directions of Cu(111) surface. The six KS domains give rise to six satellite spots in the corresponding LEED patterns, as shown in the bottom pictures of figure 3 [37]. The morphological and structural evolution, as a function of thickness, is shown in the STM images and LEED data in figures 4 and 5, respectively. The data in these figures were acquired from Fe films grown on a Cu(111) substrate with a slight miscut angle of 1.2°. The critical thickness of the fcc → bcc transition in these Fe films is between 2.3 and 2.7 ML, as evidenced by the appearance of bcc ridges in figure 4 and the change of interlayer distance (as determined by LEED-IV) in figure 5. In the past, there has been some inconsistency in values reported for the critical thickness of the fcc → bcc transition. A thickness of 5 ML was reported for Fe growth on a flat Cu(111) substrate [37], while 1.5 ML was found for Fe on a vicinal Cu(111) substrate with an 8° miscut angle [38]. This inconsistency, however, reflects the fact that the nominal thickness is only an average value of the height of an assembly of multilayer islands. STM studies indicate that, when the local thickness of a particular island exceeds 6 ML, the morphology of that island becomes bcc-

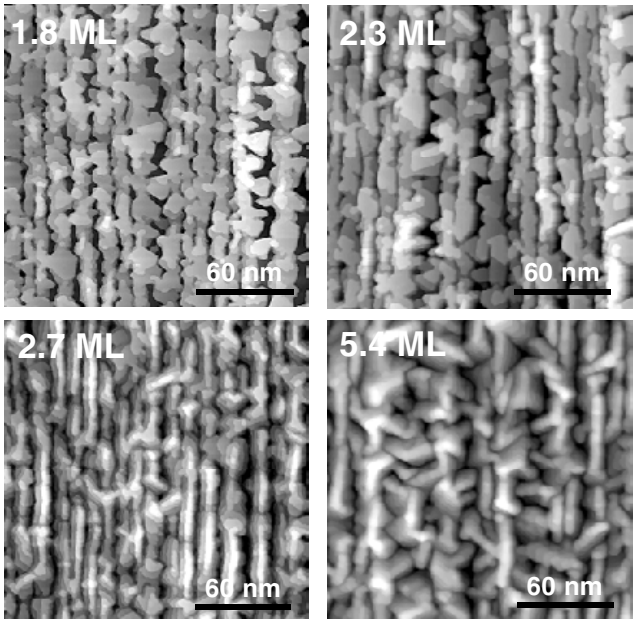

Figure 4. STM images of thermal MBE-grown Fe on Cu(111) that show the morphological change that occurs when the film undergoes an fcc to bcc structural transition between nominal thicknesses of 2.3 and 2.7 ML.

like with elongated structures. As we will discuss later, Fe adatoms have a strong preference for nucleation at the atomic step edges of a Cu(111) substrate. This implies that the height distribution of the mutilayer islands is strongly affected by the density of the substrate steps, even if the nominal thickness of Fe is unchanged. With this in mind, most of the varying results in the literature are actually consistent with each other.

The substrate temperature has a profound influence on the growth and especially the fcc $\rightarrow$ bcc transition of Fe on Cu(111). A forward-scattering x-ray photoelectron diffraction study showed that the fcc structure of Fe on Cu(111) can only be obtained when the substrate is kept warmer than 80 K during growth [39]. At temperatures lower than 80 K, epitaxy of Fe on Cu(111) cannot be properly established and the more stable bcc phase dominates the growth. At temperatures significantly above room temperature, $\sim$700 K for example, the bcc Fe phase only appears at a thickness greater than 40 ML. However, the seemingly delayed fcc $\rightarrow$ bcc phase transition is a direct consequence of Fe–Cu interdiffusion. In fact, Fe–Cu interdiffusion already occurs to some extent at room temperature [40].

2.2. Magnetism

The thermal MBE grown Fe/Cu(111) films have consistently been found to be in a low-moment phase, in stark contrast to the high-moment phase observed in thermal MBE grown Fe films on the Cu(100) surface [41]. Early experiments on surface-coated Fe/Cu(111) films, prepared in a 10^{-8} Torr vacuum, showed that the magnetic moment of the fcc Fe is only about 0.58 μ_B [42]. Electron-capture spectroscopy measurements on UHV-grown, uncoated films detected short-range ferromagnetic order in films thinner than 2 ML [43], which is consistent with the multilayer island morphology and the discontinuity of the films shown in figure 2. More recently, the thickness dependence of magnetism of Fe/Cu(111), measured by surface

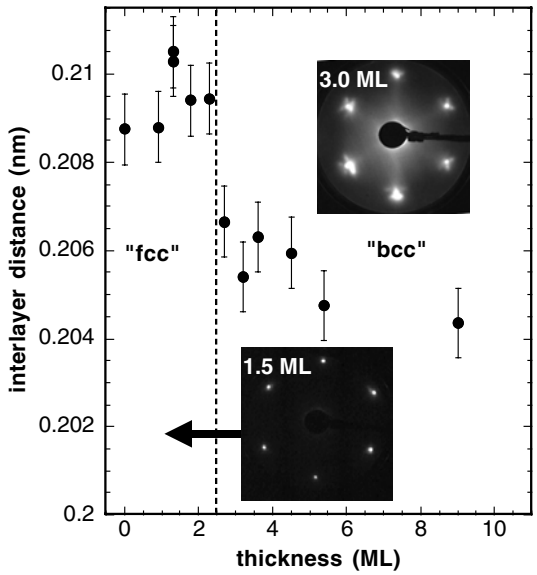

Figure 5. Plot of the vertical lattice constant of thermal MBE-grown Fe films as a function of thickness. A sharp and sudden drop in this lattice constant is observed at a thickness of 2.5 atomic layers, which corresponds well to the thickness at which the ridge-like structures appear in the STM images in figure 4.

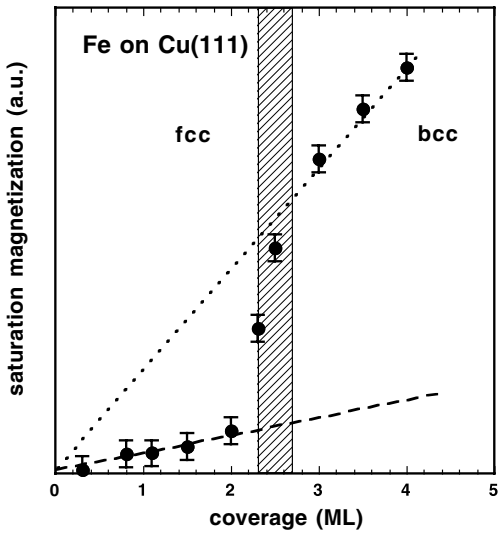

Figure 6. Thickness dependence of the surface SMOKE signal observed when the magnetization of thermal MBE-grown Fe films is saturated in a direction perpendicular to the Cu(111) surface. The data show that a low-moment to high-moment magnetic transition occurs at the same thickness as the structural changes discussed in figures 4 and 5.

magneto-optical Kerr effect (SMOKE), gave strong evidence that the uncoated fcc Fe has a considerably smaller net magnetic moment than that of bulk bcc Fe [44]. Figure 6 shows the saturation polar Kerr intensity as a function of Fe/Cu(111) thickness. Apparently, the positive slope of Kerr intensity as a function of thickness takes two distinctly different values in the fcc

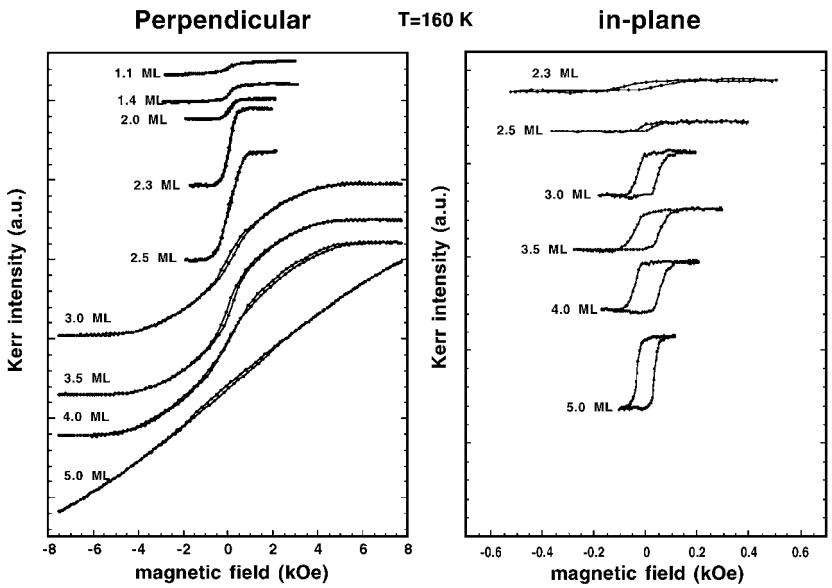

Figure 7. Hysteresis loops obtained with the SMOKE for thermal MBE-grown Fe films of various thicknesses. The data indicate that the easy axis of magnetization of these films rotates from the perpendicular to the in-plane direction at the thickness at which the previously discussed structural transition happens. The vertical scale of the plot of the in-plane loops has been reduced relative to that of the plot on the left since the intensity observed in the longitudinal Kerr effect is smaller than what is seen in the polar geometry.

and bcc regime, with the bcc slope being nearly four times larger. Assuming that the saturation Kerr intensity is roughly proportional to the net magnetic moment of the sample, one would conclude that the MBE-grown fcc Fe/Cu(111) has a moment of the order of 0.5 μ_B. A number of photoemission studies show signs of smaller exchange splitting for the films in the fcc regime than that of the films in the bcc regime [45–47]. This is consistent with the observation of a low-moment phase. Recently, further details regarding the nature of this low-moment phase have been revealed by an x-ray magnetic circular dichroism (XMCD) study [48], which will be discussed in section 4.

The fcc $\rightarrow$ bcc structural transition not only induces the low-moment to high-moment magnetic transition, but also drives a spin reorientation transition. Figure 7 shows the side-by-side comparison of polar and longitudinal MOKE hysteresis loops of the same Fe/Cu(111) sample measured in figures 4 and 5. At thicknesses below 2.3 ML, only polar loops can be measured. The polar loops generally have a very low remanence, reflecting the reduced thermal stability of the multilayer islands in the system. When the thickness is higher than 2.3 ML, in-plane hysteresis loops become detectable, while the saturation field for polar loops increases rapidly with increasing thickness. Well-defined square hysteresis loops are measured in the in-plane direction when the films are in a bcc structure.

3. Laser MBE growth: two-dimensional ultrathin films

3.1. Laser MBE growth

While Fe/Cu(111) films grown with conventional molecular beam epitaxy show interesting features such as a low-moment fcc Fe phase and a perpendicular to in-plane spin reorientation, the multilayer island morphology does not have a well-defined dimensionality and is thus not

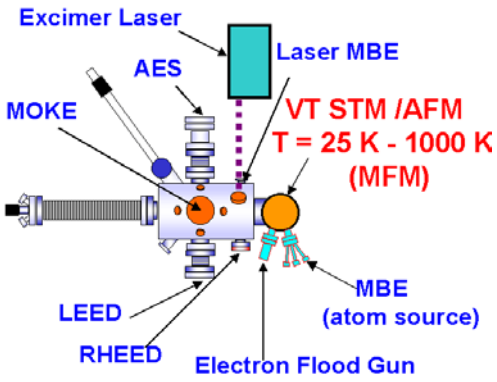

Figure 8. Schematic showing how laser MBE can be incorporated into a surface-analysis system. The laser is directed through a window and into the vacuum chamber where it ablates a target material onto a substrate that is held nearby.

ideal for studying the effect of spatial confinement on magnetism. In the last decade, a number of techniques have been developed for inducing the self-assembly of high quality magnetic nanostructures on a given template. In this section we will discuss a very powerful method for growing two-dimensional ultrathin films: laser molecular beam epitaxy.

Laser MBE essentially incorporates most of the growth principles of traditional pulsed laser deposition (PLD). In PLD, a powerful, nanosecond-pulsed excimer laser is focused onto a target. After a complex laser–solid interaction [49], a plasma plume is generated from the target and expands quickly toward the substrate. The plasma plume consists mainly of neutral atoms from the target that have a relatively moderate energy ($\sim$1 eV), plus a small fraction of ions whose energy can be as high as $\sim$100 eV. A remarkable feature of PLD is that it yields a deposition rate (during each laser pulse) of the order of 10^6 ML min^{-1} or higher, which is nearly 6 orders of magnitude higher than that of thermal MBE. This high deposition rate, according to growth theory [50, 51], tends to enhance the nucleation density, which in turn favours two-dimensional growth. This mechanism is basically similar to the so-called reentrant growth at low substrate temperatures, which also leads to high nucleation densities. Attempts to produce smooth Fe films using conventional MBE at low substrate temperatures, however, fail since Fe forms in the bcc structure from the initial stages of growth [39]. Once the bcc structure forms, Fe films will not grow two-dimensionally, or in a layer-by-layer mode, because of the large lattice mismatch between bcc Fe (of any surface orientation) and fcc Cu(111). The typical rough morphology of the bcc Fe on Cu(111) has already been shown in figure 5.

The features that distinguish a laser MBE system from a PLD system include the ultrahigh vacuum environment and the use of reflection high-energy electron diffraction (RHEED) to monitor the growth of individual atomic layers in real time. Figure 8 shows a schematic of a typical laser MBE system that has been integrated into a surface analysis chamber at Oak Ridge National Laboratory that is equipped with a number of other state-of-the-art tools for *in situ* characterization of film morphology, structure and magnetism. The combination of layer-by-layer RHEED intensity oscillations and STM analysis of layer fillings is by far the most accurate method for thickness calibration. It was shown recently that such a reliable thickness calibration method played a critical role in the determination of the hotly debated antiferromagnetic spin structure of the fcc Fe/Cu(100) system [52].

With the help of the laser MBE growth, nearly ideal layer-by-layer growth of fcc Fe films can be achieved, which is in stark contrast to the multilayer island morphology of the Fe/Cu(111) produced by thermal MBE. The surface morphology of a single atomic layer of

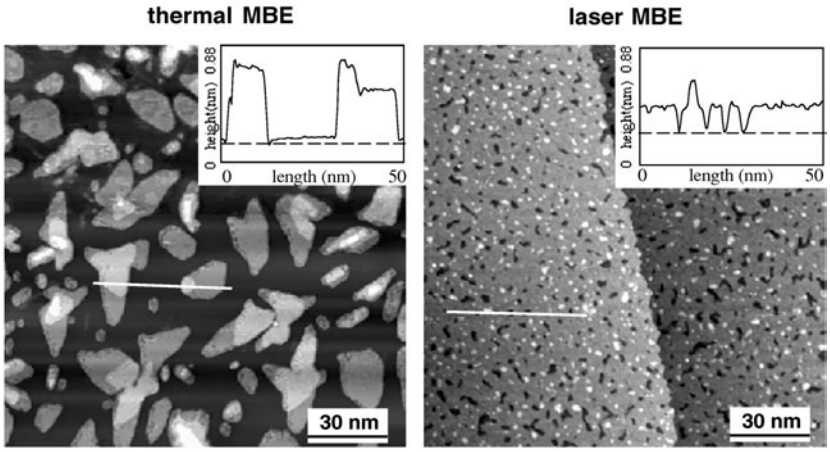

Figure 9. STM images that allow us to compare the morphologies of a single atomic layer of Fe as grown on Cu(111) with thermal MBE (left) and laser MBE (right). The laser MBE-grown film is a nearly perfect atomic layer. A substrate step runs from top to bottom through the centre of the image on the right.

Fe/Cu(111) grown by laser MBE and thermal MBE is compared in figure 9. Both films were prepared at an identical substrate temperature of 220 K. The thermal MBE film, as discussed earlier, exhibits typical multilayer island morphology that leaves a considerable amount of Cu substrate uncovered. The laser MBE Fe film, at nominal thickness of 1 ML, covers about 95% of the substrate, which can be considered as a nearly perfect monolayer film. This two-dimensional layer-by-layer growth persists up to a film thickness of 6 ML, above which an fcc $\rightarrow$ bcc structural transition occurs [53]. As we have discussed earlier, for the thermal MBE-grown Fe/Cu(111), the bcc structure starts to form locally in multilayer islands that are 6 ML high. The consistency of the fcc $\rightarrow$ bcc critical thickness for the thermally deposited and laser MBE-grown Fe/Cu(111) films implies that 6 ML and below is the thickness range in which the fcc phase of Fe is stable on a Cu(111) substrate.

3.2. Correlation between structure and magnetism

Laser MBE-grown Fe/Cu(111) films exhibit multiple magnetic phase transitions. Unlike thermal MBE-grown Fe/Cu(111), the laser deposited films appear to have a high-moment phase when the thickness is less than 3 ML. Above 3 ML, this high-moment phase transforms into a low-moment phase, and eventually becomes a high-moment phase again once the films complete the fcc $\rightarrow$ bcc structural transition ($>$6 ML). Figure 10 shows the magnetic phase diagram for laser MBE-grown Fe/Cu(111) films. The change in saturated polar Kerr intensity with thickness for films that are thinner than 3 atomic layers is more than 3 times higher than that for films thicker than 3 ML. At thicknesses beyond those shown in the plot, when the films become bcc (above 6 ML), the slope of the Kerr intensity almost recovers the original value (not shown here). Again, assuming the Kerr intensity is proportional to the net moment of the films, one would conclude that at low thicknesses ($<$3 ML), the laser MBE-grown fcc Fe/Cu(111) films have a high magnetic moment which more or less equals the bcc Fe moment (2.2 μ_B). This high-moment phase transforms into a low-moment phase of 0.7 μ_B when the film thickness exceeds 3 ML. To date, the nature of the low-moment phase, i.e. whether it comes from a low-spin ferromagnetic phase, a ferrimagnetic phase or even a noncolinear spin structure [54], is undetermined.

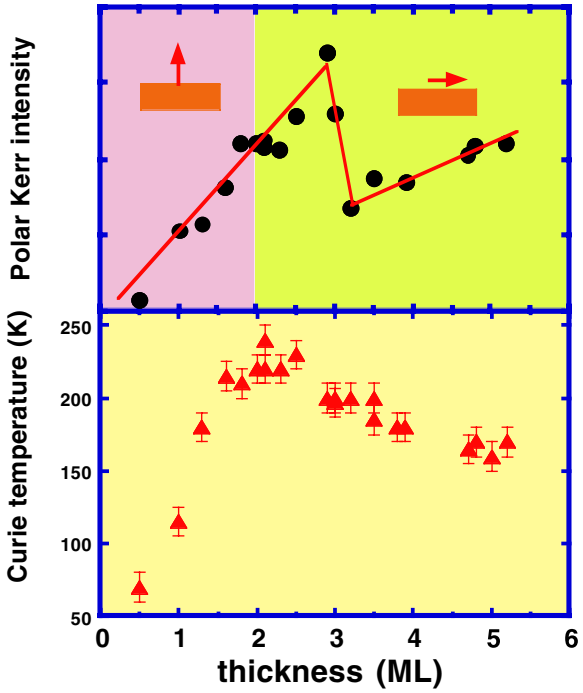

Figure 10. The upper plot shows the magnetization of the laser MBE-grown films as a function of thickness. The spin reorientation that occurs at a film thickness of 2 ML does not appear to be associated with the high-moment to low-moment transition that is observed at a thickness of 3 ML. The lower plot shows the thickness dependence of the Curie temperature of these films.

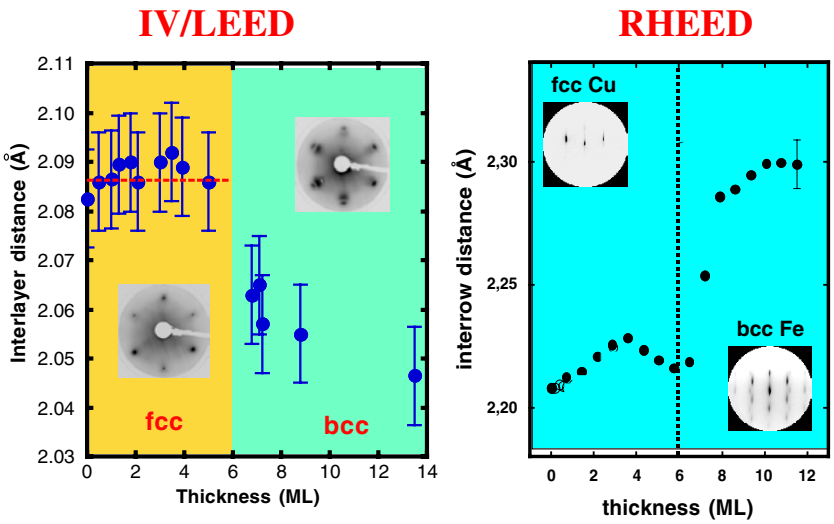

Figure 11. Structural measurements of laser-deposited Fe films that show a sharp decrease in the vertical lattice constant (left) and a sudden increase in the in-plane lattice constant (right) at a thickness of 6.0 atomic layers. The decrease of the in-plane lattice constant between 4 and 6 ML may be associated with the high-moment to low-moment transition, as discussed in the text.

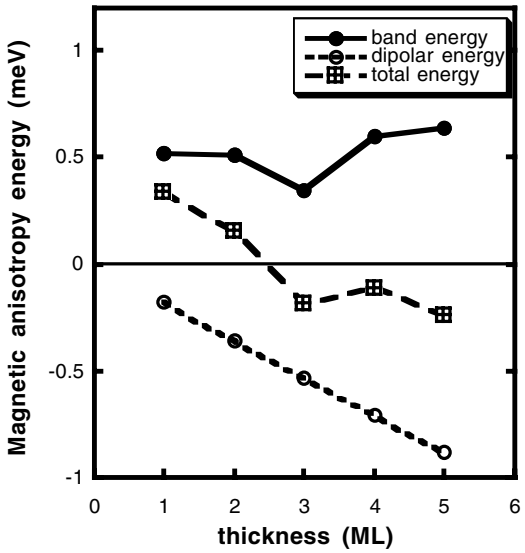

Figure 12. Plot of the results of an *ab initio* calculation of the various contributions to the magnetic anisotropy of laser MBE-grown Fe films on Cu(111). The change in sign of the total anisotropy energy that is found at 2.5 ML indicates that a perpendicular to in-plane spin flop should occur at that thickness. This is in good agreement with experimental observations (courtesy of B Ujfulussy).

Detailed structural analysis indicates that the high-moment to low-moment phase transition is associated with a slight change of lattice constant of the Fe films. Figure 11 shows the thickness-dependent vertical (a) and lateral (b) lattice constants of the laser MBE-grown Fe/Cu(111) films. The vertical lattice constant, or the interlayer distance, was determined by LEED-IV measurements. It does not change throughout the entire fcc thickness regime. The lateral lattice constant, or the inter-row distance, was determined by RHEED. It initially increases with thickness, reaching a maximum between 3 and 4 atomic layers. The distance between rows then decreases with increasing thickness, before it adopts a much larger value in the bcc regime (>6 ML). Figure 11(b) clearly shows that the thinner Fe films (<4 ML) have a larger inter-row distance than that of the thicker Fe films (between 4 and 6 ML). The initial increase of the inter-row distance likely reflects the fact that some of the electrons that contribute to the diffraction pattern actually diffract from the Cu substrate itself. This effect would make the measured value of the Fe lattice constant appear smaller during the initial stages of growth, and becomes less important with increasing thickness, since the penetration depth of a RHEED beam is typically no more than 2–3 atomic layers. The average inter-row distance peaks at 3–4 ML, at which the contribution from the substrate is negligible. The subsequent decrease of the inter-row distance, however, has to be attributed to the intrinsic structural behaviour of the Fe films, since the presence of the substrate no longer affects the measured values. With this argument, and the information from both figures 11(a) and (b), one may conclude that, in the fcc thickness regime, the atomic volume of Fe films is slightly larger at low thicknesses (<3–4 ML) than it is when the films are between 4 and 6 ML thick. Considering the well-known fact that a larger lattice constant favours a larger magnetic moment for fcc Fe [30], the lattice constant decrease between 4 and 6 ML in figure 11(b) provides a plausible explanation of the high-moment to low-moment phase transition for the laser MBE-grown films.

A perpendicular to in-plane spin reorientation transition was also observed in the laser MBE-deposited Fe/Cu(111) films. This occurs at about 2 ML and thus is not associated with

either the fcc → bcc structural transition (6 ML) or the high-moment to low-moment magnetic transition (3 ML) in this system. This is in stark contrast to the spin flop transition observed in thermal MBE-grown Fe/Cu(111), which is originated by an fcc → bcc structural phase transition. An *ab initio* calculation, based on the fully relativistic screened KKR method, was recently made by Uljfulussy *et al* [55], showing that this spin flop transition is governed by the balance between perpendicular magnetocrystalline anisotropy and in-plane shape anisotropy. As shown in figure 12, the magnetic anisotropy band energy (magnetocrystalline anisotropy) has positive values that favour perpendicular magnetization. The weak thickness dependence implies that the main contributions to this energy term come from the surface and interface. The demagnetizing energy (shape anisotropy), as is the case in all magnetic ultrathin films, has negative values and increases linearly with thickness. The total anisotropy energy, i.e. the sum of the band energy and demagnetizing energy, changes its sign from positive to negative at a thickness of about 2.5 ML, predicting a magnetization reorientation at that thickness. This is in good agreement with the experimental findings.

The unusual thickness dependence of the Curie temperature (T_C) of the Fe ultrathin films, which seems to have a maximum at about 2 ML (figure 10), is a puzzle that is still not understood. Although some kind of non-monotonic behaviour of T_C is expected due to the magnetic phase transitions, there are two major surprises regarding its thickness dependence in this system. First, T_C starts to decrease at 2 ML, a thickness at which the Fe films are still uniformly in a high-moment phase. Second, T_C monotonically decreases with increasing thickness above 2 ML. At that thickness, this behaviour cannot be attributed to the onset of the low-moment phase or to the spin reorientation. Interestingly, the first behaviour was also observed in the Fe/Cu(100) system, and was understood to be caused by a temperature-induced structural transition during the T_C measurement [56]. Temperature-induced structural transitions have not been carefully examined so far in the Fe/Cu(111) system and cannot be used to explain the totally unexpected, monotonic decrease of T_C. Further structural and spin-polarized electronic information is needed to understand the abnormal behaviour of T_C in this system.

4. Step decoration on vicinal surface: quasi-one-dimensional stripe array

4.1. Formation of one-dimensional nanostructures

One-dimensional (1D) systems have intrigued scientists for many years. In the years before powerful and cheap computing, 1D models, where analytical solutions existed, often appeared to be the best theoretical vehicle for studying many phenomena. Physics in one dimension is quite different from physics in two or three. For example, in 1D, there can be no phase transitions or long-range order [57] nor can there be electrical conduction because all electronic states are localized [58]. We live, however, in a space of three dimensions, so great care must be used in applying the theorems of 1D to experimental examples of one-dimensional systems (quasi-one-dimensional).

To date, these experimental model systems have included two distinctly different classes of materials: (1) single-crystal compounds that consist of magnetic ion chains and (2) magnetic nanowire or nanostripe arrays. While the former provides an interesting arena for the study of 1D physics [59], the latter has the potential to become technologically relevant and thus has received a great deal of attention [60–62], particularly after the promising work by Elmers *et al* [4] on Fe stripes grown on W(110) substrate.

In Elmers' investigations, Fe stripes were prepared by exploiting a process called step-flow growth. The underlying mechanism for step-flow growth is very similar to that for the

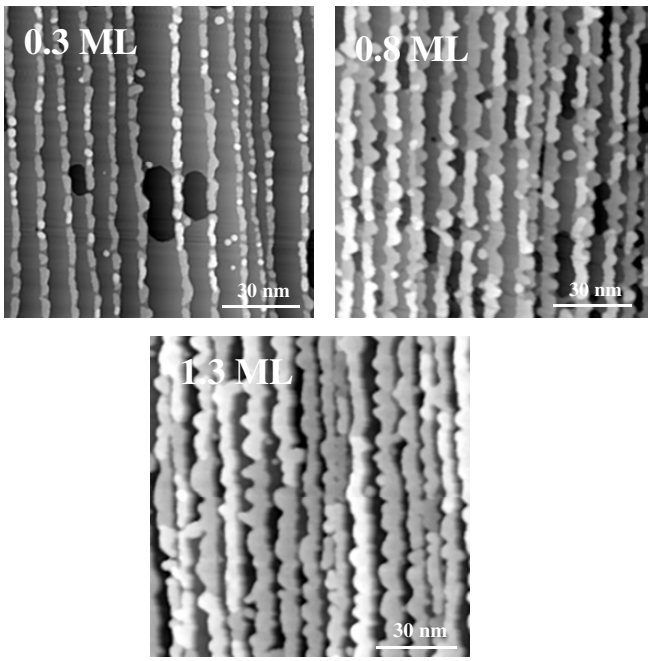

Figure 13. Series of STM images that highlight the step-edge decoration of Fe on Cu(111). The width and separation of the Fe wires can be tuned by varying the amount of Fe dosed.

annealing of a freshly cleaned metallic single-crystal substrate after ion sputtering. Annealing drives surface atoms to the step edges via thermal diffusion. In the case of Fe/W(110), the Fe atoms were first deposited on tungsten at room temperature, and then annealed to 750 K. This annealing temperature is high enough to allow thermal diffusion of Fe atoms but low enough to keep the steps of W(110) substrate immobile. During the anneal, Fe atoms flow to align along the step edges and eventually, if the amount of iron dosed is low enough, form isolated, quasi-one-dimensional stripes. Very recently, FeCo alloy stripes have been made using a similar recipe [63].

Step-flow growth is a rather general phenomenon that can be used to prepare one-dimensional stripes, provided that the adatoms in the system at hand have a strong tendency to wet the substrate, and that the substrate atoms and deposited magnetic atoms do not intermix with each other at the annealing temperature. This generally requires that the substrate has a considerably higher surface free energy than that of the deposited material, and that the miscibility between the two materials is low. These criteria are not met in the Fe/Cu(111) system, since the surface free energy of Fe is considerably higher than that of Cu [64], which leads to a significant Fe–Cu interdiffusion at elevated temperatures [39]. Luckily, in this particular system, Fe adatoms have a strong preference to nucleate at the upper terrace sites of the step edges even at room temperature or slightly below. To exploit this step decoration effect, we chose a Cu(111) substrate with a small miscut angle of 1.2° in order to grow parallel Fe stripes. This vicinal, or miscut, surface has an average terrace width of about 10 nm, which is narrow enough to allow almost all Fe adatoms to nucleate at the step-edge sites. Figure 13 shows STM images taken from several of these Fe/Cu(111) stripe arrays with various nominal thicknesses. Depending on the thickness, the stripes are typically 1–2 ML high and 2–5 nm wide. This step decoration effect has also recently been used to fabricate Fe nanowires on an insulating NaCl(100) substrate [65].

In addition to methods that utilize stepped surfaces, alternative techniques for growing 1D chains or stripes include the self-assembly of lateral superlattices in bimetallic systems, and shadow deposition on grating templates. Tober *et al* [66] have shown that thin films of CoAg or FeAg alloys grown on Mo(110) consist of alternate 1D stripes of Co (or Fe) and Ag, forming an array of Q1D magnetic multi-wires. Sugawara and co-workers [67] have prepared Fe nanowires using shadow deposition on a grating NaCl(110) template. Electrochemical [68] and electroless [69] deposition of nanowires in spatially ordered channels in nanoporous materials has also been explored.

4.2. Quasi-one-dimensional magnetism

As mentioned in the previous section, because of the absence of long-range order, ferromagnetism should not exist in a truly 1D system with short-range interactions. The quasi-one-dimensional Fe/W(110) stripes, nevertheless, seem to show a ferromagnetic behaviour which is explained as a result of their in-plane magnetic anisotropy and their long-range dipolar interactions [70]. (Since these stripes are not perfect single atomic chains and the chains have been found to interact with each other via dipolar coupling, we refer to this system and similar systems as quasi-one-dimensional.) This dipolar interaction, however, should not favour ferromagnetism in the Fe/Cu(111) stripe arrays whose easy magnetization axis is along the surface normal.

Indeed, the Fe/Cu(111) stripes show distinctly different behaviour than the stripes in the Fe/W(110) system. Figure 14(a) displays magnetic hysteresis loops, measured by polar MOKE, for an Fe/Cu(111) stripe array made from a nominal Fe dose of 0.8 atomic layers. No magnetic signal was observed in the longitudinal geometry, whether the external field was applied parallel or perpendicular to the stripes, indicating that the easy magnetization axis is along the surface normal. Figure 14(b) shows the temperature dependence of the saturation magnetization (M_s) and remnant magnetization (M_r) of the Fe stripes. With increasing temperature, M_s is rather stable compared to M_r, which decays quickly. Upon further increase of the temperature above 250 K, M_s drops sharply, indicating that the system becomes non-magnetic. The dramatically different temperature dependences of M_s and M_r give a first hint that the Fe/Cu(111) stripe arrays are by no means a conventional ferromagnetic system.

This is further supported by the strong time dependence of the magnetization of the Fe stripes. Figure 15 shows the time dependence of the magnetization of the same 0.8 ML Fe/Cu(111) stripe array. The zero level defines the demagnetized state of the Fe stripes. After switching on the external field ($\sim$0.6 T) along the surface normal, the magnetization of the stripes quickly saturates. When the field is removed, at a low temperature of about 100 K, the magnetization drops rapidly to about 70% of M_s, and then decays slowly. The slow decay of the magnetization at 100 K guarantees the apparent ferromagnetic behaviour of the system during the time in which MOKE hysteresis loops are recorded. At a higher temperature of about 160 K, the magnetization relaxation process becomes significantly faster.

The strong time dependence of the magnetization suggests the absence of long-range ferromagnetic order in Fe/Cu(111) stripe arrays. However, short-range ferromagnetic order does exist since the system can be saturated by a moderate field ($<$0.8 T). Based on these observations, we explain the magnetic behaviour in terms of a model involving interacting Ising spin blocks [71]. A schematic picture of the model is shown in figure 16. Within an individual stripe, the relevant parameters include the anisotropy constant K_1, the volume of the spin block units (V_0) and the exchange coupling constant between adjacent spin blocks (J). The spins inside each block are aligned parallel to each other, but due to thermal activation there

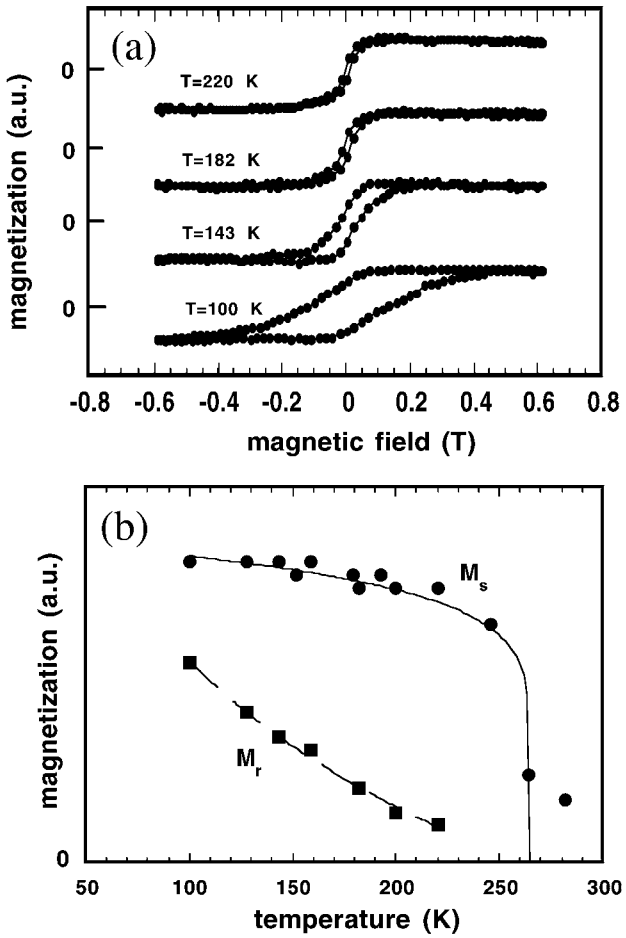

Figure 14. (Top) Temperature dependence of polar SMOKE hysteresis curves observed in nanostripes made from 0.8 ML of Fe on Cu(111). (Bottom) Temperature dependence of the saturation (M_s) and remnant (M_r) magnetization.

is no long-range ferromagnetic order amongst all spin blocks. The fact that the magnetization curves of the Fe films show hysteresis indicates that the films are in a 'frozen' or 'blocked' superparamagnetic state. The blocking temperature, T_b, can be estimated from the vanishing of the coercivity, which is about 200 K for the 0.8 ML Fe stripes. Above T_b the system behaves like a typical superparamagnet in that it exhibits no hysteresis and has essentially the same M_s at all temperatures in an external field. At even higher temperatures, above 270 K, the individual spin blocks become magnetically disordered as indicated by the vanishing of M_s (figure 14).

The magnetization curves of the Fe stripes can be understood using a generalized one-dimensional Ising model for a set of spin blocks [72]:

$$\frac{M}{M_s} = \frac{\sinh(h/k_BT)}{\sqrt{\sinh^2(h/k_BT) + \exp(-4J/k_BT)}} \tag{1}$$

where $h = \mu_0 M_S H V_0$. To understand the hysteretic behaviour of the Fe stripes (figure 14), it is necessary to include non-equilibrium effects which may be represented by the well-known

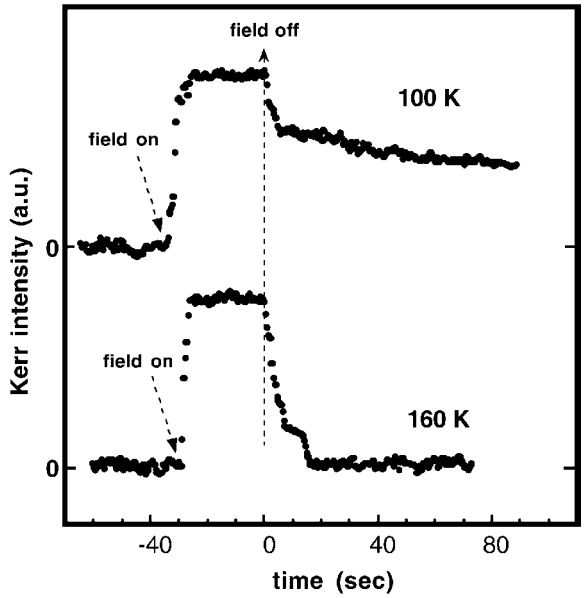

Figure 15. Time dependence of the magnetization of the nanostripes. The magnetization of the samples was saturated with a 30 s field pulse. When the applied field was removed (at time = 0), the magnetization was allowed to relax. The slow decay of the remnant signal shows that the shape of the loops and curves in figure 14 could vary greatly, depending on the duration of the measurements.

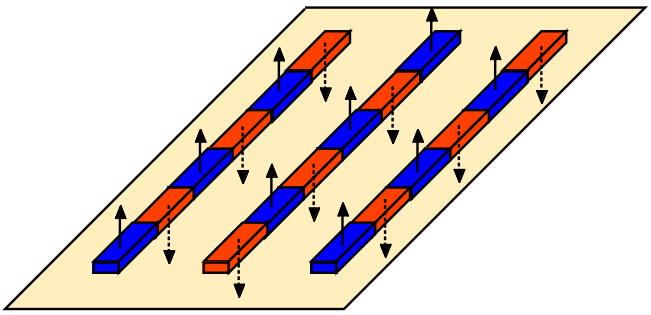

Figure 16. Schematic of the Ising spin blocks in the nanostripes. The spins of all atoms in a particular spin block are parallel and point either into or out of the surface.

Glauber transition rate. After some calculation one obtains for small J and narrow hysteresis loops

$$\frac{M}{M_s} = \left(1 + \frac{2J}{k_BT}\left(1 - \tanh^2\frac{h}{k_BT}\right)\right)\tanh\frac{h}{k_BT} - \frac{r}{\Gamma}\left(1 - \tanh^2\frac{h}{k_BT}\right)\left(1 - \frac{4Jr}{\Gamma k_BT}\left(1 - 4\tanh^2\frac{J}{k_BT}\right)\right) \tag{2}$$

in which $\Gamma = \Gamma_0 \exp(-\frac{V_0 K_1}{k_B T})$ and $r = \frac{1}{M_s}\frac{\partial H}{\partial t}$. Using equation (2) we have fitted four representative hysteresis loops: 0.3 ML at 50 K, 0.6 ML at 163 K, 0.8 ML at 182 K and 200 K, respectively. For each of the four curves, the sweeping rate r was about 0.04 T s^{-1}. The fitted curves, as well as the fitting parameters (K_1, J and V_0), are shown in figure 17. The

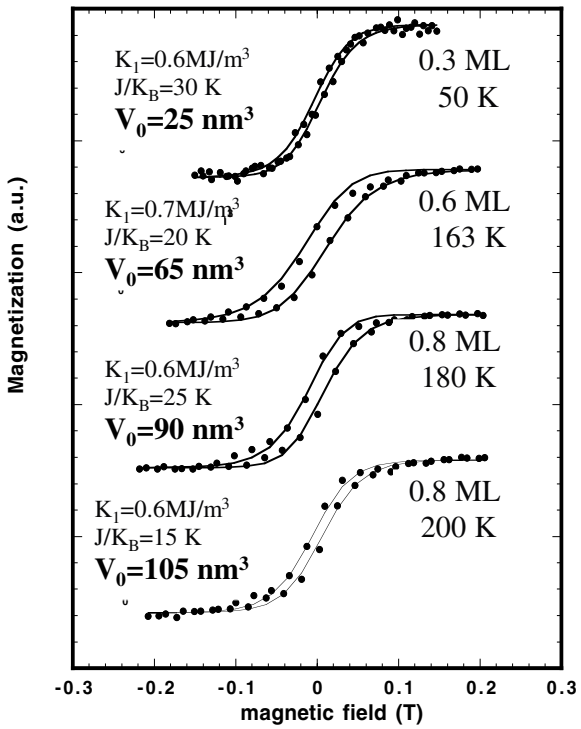

Figure 17. Thickness dependence of SMOKE hysteresis curves (dots) for the nanowires, along with the fitting provided by the spin block model (full curves). Note that the volume of spin blocks increases with increasing thickness.

anisotropy constant K_1 is in the range between 0.55 and 0.80 MJ m^{-3}. These values are an order of magnitude larger than the bulk anisotropy of α-Fe (0.05 MJ m^{-3}), indicating that the surface anisotropy is the dominant contribution to K_1. The fitted V_0 increases with increasing thickness, which is consistent with the STM images (see figure 13) that show that the segments in the stripes become longer with increasing thickness. Moreover, V_0 is also compatible with the actual geometry of the segments. Taking the average width of 4 nm and height of 0.2 nm, for the 0.3 ML stripes ($V_0 = 25$ nm^3) we estimate the length of the block-spin unit to about 30 nm. This roughly agrees with the average length of the segments in the 0.3 atomic layer stripes shown in figure 13.

Therefore, the fit in figure 17 shows that the model gives a fair description of magnetism in these stripe arrays. The fact that J, the strength of the block–block coupling, has a non-zero value indicates the Fe stripes are different from a system consisting of isolated clusters or islands, in which J should be zero. The restriction of the model to small J is reasonable for small Fe coverages, because, physically, the smallness of this value reflects the fact that the width of the stripes is not constant but has pronounced minima, or small 'kinks' at which the switching of the magnetization of adjacent spin blocks is relatively easy. There is, in fact, no major difficulty in generalizing equation (2) to accommodate large values of J, but then some other processes, such as domain-wall motion along the stripes, would complicate the analysis.

The temperature dependence of the magnetization of the Fe stripes has been recently calculated with Monte Carlo simulations [73]. The calculation indicates that the exchange interaction between spin blocks within the Fe stripes is at least more than an order of magnitude smaller than it is in bulk Fe, and that some kind of magnetic disorder may also exist in the Fe

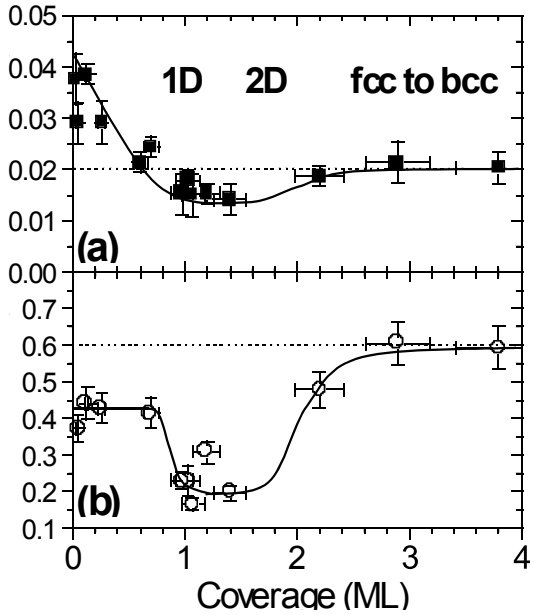

Figure 18. The thickness dependence of the orbital (a) and spin (b) contributions to the magnetic moment of the nanowires, as determined by XMCD (courtesy from P Ohresser).

stripes. The dipolar interaction between the Fe stripes is negligible, as far as the temperature dependence of the magnetization is concerned. The roles of some other interactions such as indirect exchange coupling through the substrate, however, have not been investigated so far.

Finally we comment on the magnetic moment of the Fe stripes. The MOKE measurements [44], as mentioned earlier, showed that the Fe stripes have a low magnetic moment of about 0.5 μ_B. A recent XMCD study gives a more reliable number of $0.7 \pm 0.2\ \mu_B$ for the Fe stripes, which essentially agrees with the MOKE results. Interestingly, the XMCD work further showed that before the step-decorated Fe atoms form continuous stripes (<0.8 ML), their magnetic moment is about $1.4 \pm 0.2\ \mu_B$. Figure 18 shows the thickness dependence of orbital and spin moment of Fe stripes on Cu(111). Assuming the number of holes per Fe atom in the stripes is close to that of bulk Fe (3.39), the spin moment clearly shows signs of a phase transition, from 1.4 to 0.7 μ_B at about 0.8 ML thickness, above which the stripes become continuous. Although the origin of this phase transition is yet to be investigated, one could envision that a slight change of lattice constant, which is associated with the formation of continuous stripes, plays an important role in this phase transition.

5. Buffer layer assisted growth: Fe dot assemblies on Cu(111)

5.1. Formation of quasi-zero-dimensional clusters of Fe on Cu(111)

Compared to the synthesis of the other nanostructures highlighted in this review, the growth of isolated quantum dots presented the biggest challenge. In fact, there are, to date, no published reports on quasi-zero-dimensional quantum dots of Fe on copper, despite the fact that there is fundamental interest in the effect of three-dimensional confinement on fcc Fe and in the application of magnetic quantum dots as a high density data storage medium. Based on

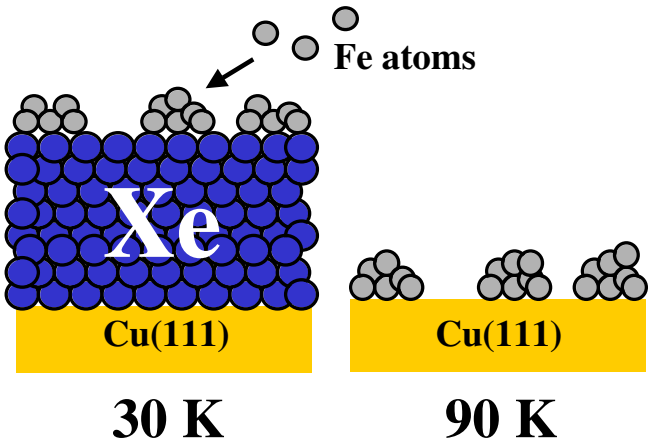

Figure 19. A schematic picture depicting the various steps of the buffer-layer-assisted growth process.

the vast body of work on the growth of Fe on copper, direct deposition of iron atoms on this surface does not yield quantum dots no matter which set of growth parameters is used. However, the recent and timely introduction of a growth method called 'buffer-layer-assisted growth' (BLAG) [74], which successfully produced quantum dots of Ag on silicon, has made it possible to grow and study isolated Fe dots on copper.

The BLAG method involves two crucial steps:

(1) Quantum dots are formed on top of an inert gas buffer layer that has been frozen onto a substrate.
(2) The buffer layer is evaporated away, allowing the formed quantum dots to land on the substrate.

The first step of the process is rather straightforward since, due to the low surface free energy of the inert gas layer, the deposited material tends to form clusters, rather than wet the surface. The second step is rather brutal and can drastically affect the spatial and size distributions of the original assembly of nanoparticles. Moreover, depending on the strength of the interaction between the quantum dots and the substrate, the dots formed may not be stable after landing on the surface and could subsequently decay into multilayer islands [75].

Recently, the group in Oak Ridge National Laboratory has successfully prepared Fe quantum dots on Cu(111) with the BLAG technique. A schematic picture of the growth process is shown in figure 19. The size and spatial distribution of the Fe dots can be modified by varying either the thickness of the Xe buffer layer or the dosage of Fe atoms [76]. A very intriguing idea has been proposed which involves using electronic charging during the Fe deposition to improve the size uniformity of the dots and their spatial ordering. Preliminary results have shown clear improvement of the size uniformity of the Fe dots via charging [77].

STM studies indicate that the BLAG process results in the formation of Fe quantum dots on the Cu substrate that are shaped like flattened hemispheres. The shape and size of the formed structures are strikingly stable as the sample is allowed to warm from 90 K to room temperature. Figure 20 shows the STM morphology of the quantum dots at 90 K (a) and 298 K (b). The quantum dots shown were made from 0.8 atomic layers of Fe (nominal thickness). The average height is 1.4 nm and the average width is 3.5 nm, as shown by the marked line profiles in figures 20(a) and (b). The height distribution for the quantum dots,

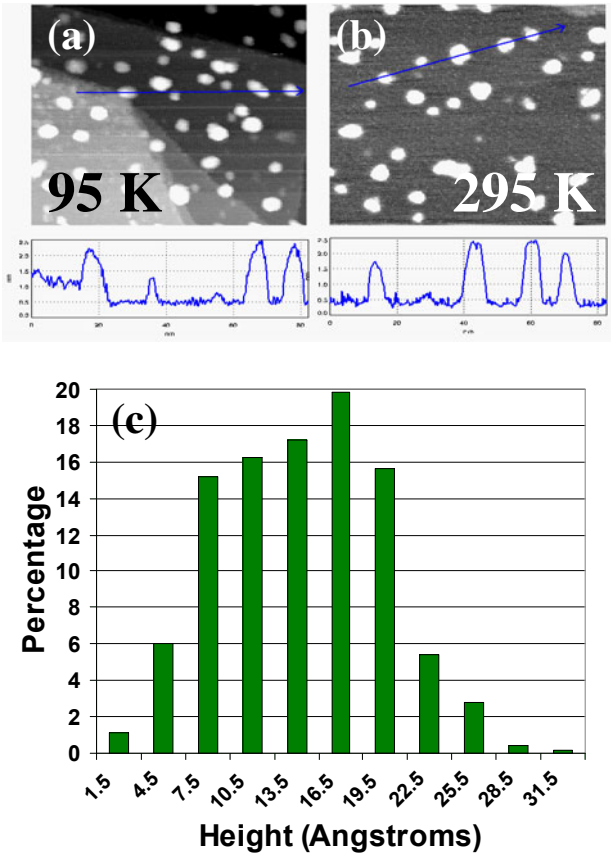

Figure 20. (Top) STM images that show that the morphology of the quantum dots is quite stable between 95 K and room temperature. (Bottom) Histogram of the heights of 685 quantum dots observed in large-area STM images.

as imaged at room temperature, is shown in figure 20(c). This distribution is not appreciably different at low temperatures.

5.2. Magnetic behaviour of arrayed dots

In situ MOKE measurements on these Fe dots have, surprisingly, revealed ferromagnetic stability at temperatures below 120 K. As shown in figure 21(a), magnetization curves were recorded with the magnetic field both perpendicular to and in the plane of the sample. The easy magnetization axis of the dots lies in the plane of the Cu(111) surface, as evidenced by the fact that magnetic hysteresis loops were observed only when the field was applied parallel to the surface. The remnant magnetization of the dot assembly is remarkably stable with respect to time, as indicated by the time-dependent magnetization measurements in figure 21(b). To perform time-dependent measurements, we first demagnetized the sample to set a zero reference level, and then saturated it with an external field applied in the surface plane. After a short period, the external field was switched off to allow for time-dependent measurements of remnant magnetization. Figure 21(b) shows that, after an abrupt initial drop, the remnant magnetization decays very slowly with respect to time. This stability of M_r in time allows us to determine the critical temperature of the Fe dots to be about 120 K, as shown in figure 22. It is not immediately clear what mechanism supports this ferromagnetic stability in the quantum

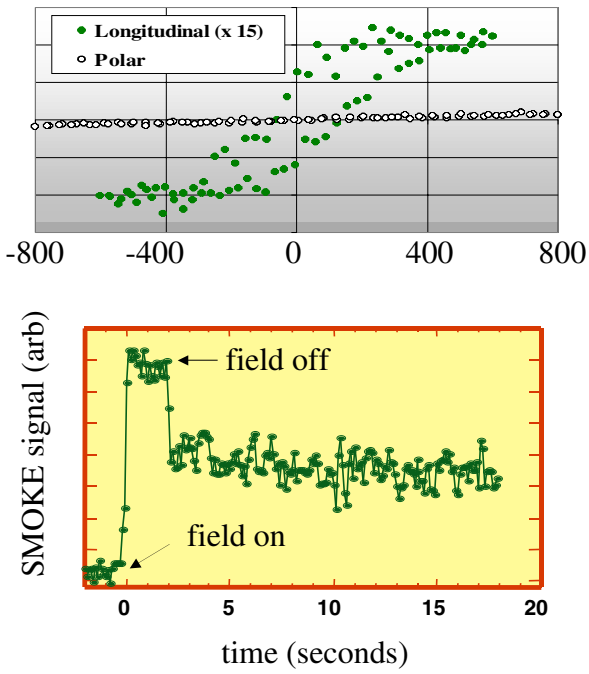

Figure 21. (Top) Longitudinal (in-plane) and polar (perpendicular) SMOKE hysteresis curves acquired from an assembly of quantum dots generated from 0.8 atomic layers of Fe. (Bottom) Time-dependent measurements of the in-plane magnetization of the quantum dot assembly. The remanent magnetization appears to be stable after a initial quick drop when switching off the external field.

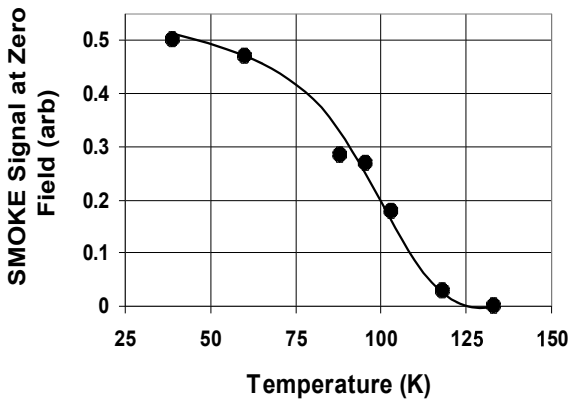

Figure 22. Temperature dependence of the remnant magnetization observed in dot assemblies made with 0.8 atomic layers of Fe on Cu(111). The remnant magnetization vanishes at about 120 K.

dots, which one would expect to exhibit superparamagnetic behaviour. As mentioned in section 4, Elmers *et al* have observed similar ferromagnetic behaviour in a system of quasi-one-dimensional Fe stripe arrays on W(110), and have attributed the ferromagnetic stability to the inter-stripe dipolar interaction.

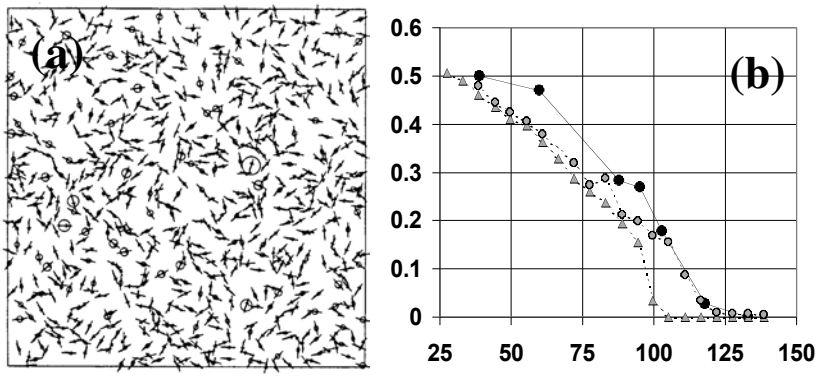

Figure 23. (a) A snapshot of the magnetization of the quantum dots at 56 K, as determined by Monte Carlo calculations. This image was generated with quantum dot size and position data from a 240 × 240 nm STM image and contains 685 individual particles. The thin lines represent the uniaxial anisotropy axes and the arrows are the projections of the particles' magnetization onto the surface plane. (b) A plot of the Monte Carlo results (grey circles and triangles) and measured data (black circles). The fitting shows that the dipolar interaction between the dots plays a significant role in the ferromagnetic stability observed in this system. Neglecting these magneto-static interactions would reduce the calculated ordering temperature by 20°.

In order to examine the relative roles played by magnetocrystalline anisotropy and the dipolar interaction in the present Fe dot assembly, Lee *et al* [78] conducted Monte Carlo simulations that calculated the temperature dependence of the remnant magnetization. These simulations used the experimentally measured positions and sizes of the Fe quantum dots as input. Each dot was modelled as a single dipole moment whose strength was determined by multiplying the bulk Fe magnetization (SMOKE studies give indirect evidence that the dots are in a high-moment phase) by the experimentally determined dot volume. Each dot was given a fixed uniaxial anisotropy axis, whose orientation was randomly assigned. The moments were initially all forced to point along a certain direction, and then the sample was allowed to relax to its remnant state under a Metropolis Monte Carlo algorithm.

With the knowledge of the positions and sizes of the Fe dots, the dipolar interaction between the dots could be uniquely determined and was therefore not a fitting parameter. Since all other dot–dot interactions were ignored, the only fitting parameter in the simulation was the magnetic anisotropy constant, K_0. Figure 23(a) shows a snapshot of the simulated magnetization of the Fe dots at 56 K, in which the sizes and positions of the dots have been taken from experimental values measured by STM. Figure 23(b) shows the experimentally measured and Monte Carlo simulated temperature dependence of remnant magnetization of the Fe dots. The experimental and simulated data agree well with $K_0 = 6.58$ times that of the bulk bcc Fe. Although the magnetic anisotropy plays the most important role for the finite remanent magnetization and the high critical temperature ($\sim$120 K), dipolar interactions also have a non-negligible influence on the critical temperature. As shown in figure 23(b), with this optimized anisotropy constant, the Monte Carlo simulation indicated that the critical temperature would shift toward lower values ($\sim$100 K) if dipolar interactions were neglected.

The large magnetic anisotropy of the Fe dots may be caused by the large surface to volume ratio of the dots. Enhanced magnetic anisotropy of this magnitude has often been observed in ultrathin films, and tends to govern the magnetization direction at low thicknesses. The situation for the surface anisotropy of the dots is much more complex, since the crystallographic orientation of the surface atoms may vary from location to location, and is generally very hard

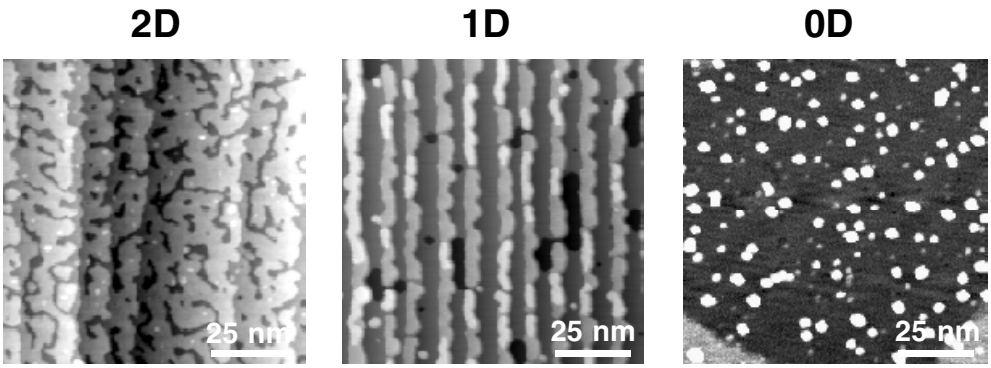

Figure 24. STM images of a film, a wire array and a dot assembly made from the same amount (0.8 atomic layers) of the same material (Fe) on the same kind of substrate (Cu(111)).

to determine experimentally. First-principles calculations of the dot anisotropy are likely to be even more challenging, although it has been shown that it is possible to calculate the magnetic anisotropy of surface step-edge atoms using Neel's spin-pair model [79].

6. Effect of spatial confinement on magnetism: direct comparison of films, stripes and dots of Fe on Cu(111)

It is typically the case that only one growth mode is thermodynamically favoured for a particular adsorbate–substrate system, and this has meant that people who have tried to make different nanostructures out of a particular material have had to reach for different templates in order to proceed. Unfortunately, it is clear that the electronic, magnetic and structural properties of monolayer thick films, nanostripes and quantum dots that consist of only a few hundred atoms are profoundly impacted by the substrates that support them. This template effect has made it extremely challenging to make direct comparisons of various magnetic nanostructures, which has, in turn, made it impossible to learn how spatial confinement of a particular material affects its magnetic behaviour. This challenge has finally been met by the aforementioned successful growth of various Fe nanostructures on a common Cu(111) substrate. In the following, we will directly compare the magnetic properties of an ultrathin film, nanostripe array and nanodot assembly prepared from the same nominal dose (0.8 atomic layers) of Fe on the Cu(111) surface. The conclusions from this comparison provide some insight into the effect of spatial confinement on magnetism.

The morphological comparison of these Fe nanostructures is found in the room-temperature (300 ± 5 K) STM images in figure 24. The Fe film consists of monolayer-high islands that just reach the percolation threshold. The Fe stripes are parallel and aligned along the substrate $\langle 110 \rangle$ direction. The stripes are typically 2–5 nm wide and are 0.2–0.4 nm high. The average centre-to-centre distance between the stripes is about 10 nm, in accordance with the average nearest-neighbour step separation of the Cu(111) substrate. The Fe dots are nearly hemispherical in shape, with an average diameter of about 3 nm.

Direct comparison of the magnetic properties of the film, stripes and dots of Fe shown in figure 24 is very surprising. The magnetic moments of the film and the dot assembly, while comparable to each other, are each about four times larger than that of the Fe stripes. Figure 25 shows their hysteresis loops measured by SMOKE at 45 K in the upper plot, and the normalized Kerr intensity vs. thickness in the lower plot. As mentioned earlier, the easy magnetization axis

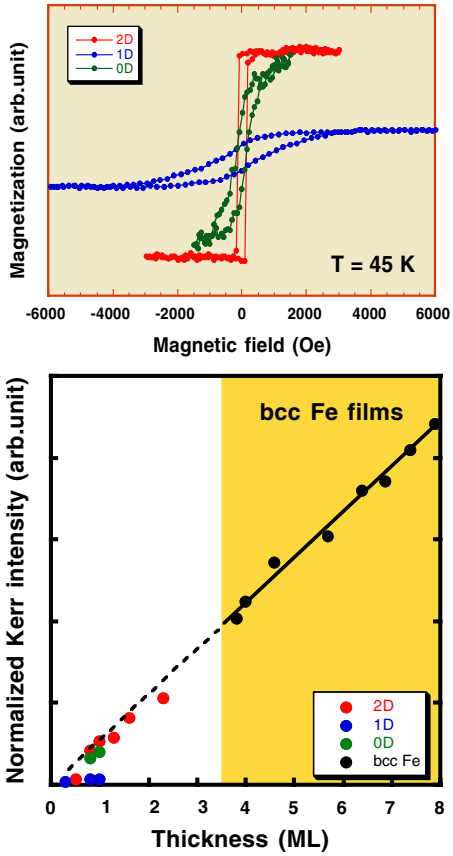

Figure 25. (Top) SMOKE hysteresis loops that correspond to the samples shown in figure 24. The easy axis of magnetization is perpendicular to the surface in the film and wire samples. The easy axis of the quantum dot assembly lies in the surface plane. (Bottom) Saturated Kerr intensity versus thickness for the samples shown in figure 24. The SMOKE signals from bcc Fe/Cu(111) films (by thermal MBE growth) are also shown for providing a reference level.

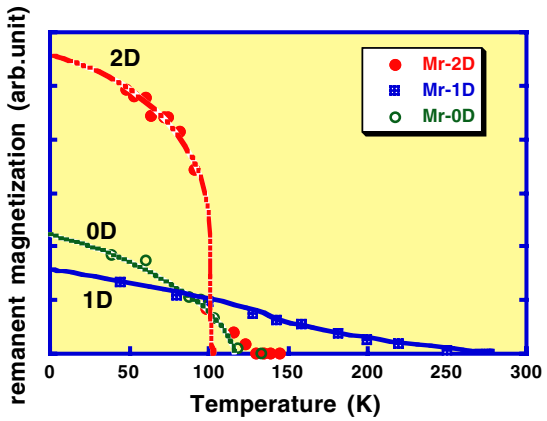

Figure 26. Plot of the temperature dependence of the remnant magnetization of the systems shown in figure 25. The 1D nanowires have a poorly defined ordering temperature since the remnant magnetization in that system is strongly time-dependent.

of the film and the stripes are perpendicular to the substrate surface, while the quantum dots have an in-plane easy magnetization axis. Consequently, the Kerr intensities were measured in the polar geometry for the film and the stripes, and in the longitudinal geometry for the Fe dots. To make the polar and longitudinal SMOKE signals comparable, they were normalized by the SMOKE intensities observed when measuring 'thick' bcc Fe films (>4 ML) on Cu(111) in the polar and longitudinal geometries, respectively. Because the thick bcc Fe/Cu(111) films are known to have a magnetic moment of 2.2 μ_B, this normalization allows us to compare the magnetic moment of the three different Fe nanostructures on Cu(111)[4]. The lower plot in figure 25 reveals that the magnetic moment of the film and the dot assembly is similar to that of bulk bcc Fe (2.2 μ_B), whereas the moment of the stripes is about 0.5 μ_B.

Along with the magnetic moment, the stability of magnetic order is also expected to be strongly dependent on spatial confinement. Textbook statistical mechanics predicts that long-range ferromagnetic order tends to become unstable in reduced dimensionality, with 1D and 0D systems described as superparamagnetic in nature. In sections 4 and 5, we have shown that both 1D stripes and 0D dots exhibit superparamagnetic blocking behaviour, although the stability of the magnetization of the 0D dots is much less sensitive to temperature change. It is interesting to ponder why this is so, particularly considering the fact that a single Fe dot has a smaller volume than an individual Fe stripe.

This issue cannot be solved using only the spin block model of the Fe stripes, as described in section 4. Under the spin block model, the relevant volume is no longer that of a single stripe, but rather that of a spin block inside each stripe. As shown previously in figure 16, the volume of each spin block in a stripe (with 0.8 ML nominal thickness) is of the order of 100 nm^3, which is still about 10 times larger than that of a single Fe dot ($\sim$10 nm^3). Although a large magnetic anisotropy is indicated by the Monte Carlo simulation for the Fe dots (section 5), the anisotropy of the Fe stripes has a comparable value as shown in section 4.

This means that we cannot describe the time-dependent magnetization of the Fe dots and stripes by treating them as non-interacting superparamagnetic entities. In section 5, we mentioned that the dipolar interaction among the Fe dots is non-negligible, and that it should help stabilize the remnant magnetization in the dots. In the Fe stripes, one would expect the dipolar interaction to have the opposite effect. Since the moments of the spin blocks are aligned perpendicular to the surface, the dipolar interaction should favour antiferromagnetic alignment of the magnetic moments in the adjacent stripes. This argument may be verified by future Monte Carlo simulations of the time dependence of the magnetization of Fe dots and Fe stripes.

The effect of temperature on the remnant magnetization is shown in figure 26. Both the Fe film and the Fe dot assembly exhibit a well-defined ordering temperature of about 100 and 120 K, respectively. Above their corresponding ordering temperature, the Fe film becomes paramagnetic, while the Fe dot assembly is superparamagnetic, with each individual dot preserving its magnetic moment, as evidenced by the observation of a nonzero saturation magnetization at a modest field ($\sim$600 Oe) at temperatures (up to 300 K) well above the ordering temperature. The Fe stripes, with their superparamagnetic nature, do not show a well-defined ordering temperature, because the remanence largely depends on the duration of the measurement, as shown in figure 15.

The non-monotonic response of the magnetic properties to the number of dimensions of spatial confinement is likely a direct consequence of the strong lattice–spin coupling in the fcc Fe system. By forming ultrathin films, stripe arrays and dot arrays on Cu(111), the Fe likely

[4] In principle, the changes of dimensionality and crystallographic structure will change the magneto-optic matrix elements and thus the measured MOKE intensity. These changes do not appear to be significant in the Fe/Cu(111) system, as evidenced by the consistent results obtained with magnetic circular dichroism by the authors in [19].

has lattice constants that are slightly different in each case, particularly since the number of step-edge atoms, which provide channels for strain relaxation, is different in the three cases. Considering the fact that a small change of lattice constant can result in a large, nonlinear response in the spin moment and the spin ordering in fcc Fe, one should expect the observation of multiple magnetic phases in various dimensionally confined nanostructures. Using copper as the substrate just amplifies this effect because a number of magnetic phases of fcc Fe are very close in energy scale at the copper lattice constant.

7. Summary and outlook

In the preceding pages we have shown that novel growth techniques can be used to prepare Fe nanostructures on Cu(111) that are smaller than the magnetic domain size in one, two and three dimensions. The growth techniques should be applicable to a multitude of systems, and similar structural and magnetic studies conducted on other systems would help to build our intuition about the effects that spatial confinement has on magnetism. This particular system, Fe on Cu(111), has shown that the magnetic properties (i.e. the ordering temperature, the time-dependent properties and the anisotropy) of a system do not change monotonically and predictably as the dimensionality of the system is reduced. In fact, the system becomes both interesting and complex! A number of unresolved issues remain, including the microscopic origin of the low-moment phase and the anomalous thickness dependence of the Curie temperature in laser MBE-grown films, and the surprising difference in the magnetic stability of the nanowire and quantum systems.

Future work on magnetic nanostructures prepared on insulating substrates could be of particular importance. In such systems, there would be true confinement of the electrons. One can imagine probing these systems in order to discover, for instance, how electron spin can influence electronic transport in a magnetic nanowire. To reach this level of study, however, a considerable amount of work remains in developing techniques for the controlled synthesis of such systems.

Acknowledgments

We are grateful to our many collaborators for their experimental and theoretical work on the Fe/Cu(111) system. In particular, we would like to thank Z Gai, P Ohresser, G A Farnan, M Klaua, A P Baddorf, J F Wendelken and J Barthel for their efforts on the growth and characterization of Fe nanostructures. We are fortunate to have had the opportunity to work with R Skomski, H K Lee, T C Schulthess, G Brown, Zhenyu Zhang, M G Stocks, B Ujfulussy and D P Landau, who provided theoretical understanding of our data. We acknowledge the sponsorships of the Laboratory Directed Research and Development Program of Oak Ridge National Laboratory, managed by UT Battele, LLC, for the US Department of Energy under Contract No DE-AC05-00OR22725, and the US National Science Foundation under contract DMR-0105232.

References

[1] Schuller I K, Kim S and Leighton C 1999 Magnetic superlattices and multilayers *J. Magn. Magn. Mater.* **200** 571–82

[2] Bader S 2002 Magnetism in low dimensionality *Surf. Sci.* **500** 172–88

[3] Sellmyer D J, Zheng M and Skomski R 2001 Magnetism of Fe, Co, and Ni nanowires in self-assembled arrays *J. Phys.: Condens. Matter* **13** R433

[4] Elmers H J, Hauschild J, Höche H, Gradmann U, Bethge H, Heuer D and Köhler U 1994 Submonolayer magnetism of Fe(110) on W(110)—finite width scaling of stripes and percolation between islands *Phys. Rev. Lett.* **73** 898–901

[5] Pratzer M, Elmers H J, Bode M, Pietzsch O, Kubetzka A and Wiesendanger R 2001 Atomic-scale magnetic domain walls in quasi one-dimensional Fe nanostripes *Phys. Rev. Lett.* **87** 127201
[6] Gambardella P, Dallmeyer A, Maiti K, Malagoli M C, Eberhardt W, Kern K and Carbonek C 2002 Ferromagnetism in one-dimensional monatomic metal chains *Nature* **416** 301–4
[7] Pietzsch O, Kubetzka A, Bode M and Wiesendanger R 2001 Observation of magnetic hysteresis at the nanometer scale by spin-polarized scanning tunnelling spectroscopy *Science* **292** 2053–6
[8] Thurn-Albrecht T, Schotter J, Kastle C A, Emley N, Shibauchi T, Krusin-Elbaum L, Guarini K, Black C T, Tuominen M T and Russell T P 2000 Ultrahigh-density nanowire arrays grown in self-assembled diblock copolymer templates *Science* **290** 2126–9
[9] Brune H, Giovannini M, Bromann K and Kern K 1998 Self-organized growth of nanostructure arrays on strain-relief patterns *Nature* **394** 451–3
[10] Woods S I, Kirtley J R, Sun S and Koch R H 2001 Direct investigation of superparamagnetism in Co nanoparticle films *Phys. Rev. Lett.* **87** 137205
[11] Majetich S A and Jin Y 1999 Magnetization directions of individual nanoparticles *Science* **284** 470–3
[12] Sun S, Murray C B, Weller D, Folks L and Moser A 2000 Monodisperse FePt nanoparticles and ferromagnetic FePt nanocrystal superlattices *Science* **287** 1989–92
[13] Fruchart O, Klaua M, Barthel J and Kirschner J 1999 Self-organized growth of nanosized vertical magnetic Co pillars on Au(111) *Phys. Rev. Lett.* **83** 2769–72
[14] Himpsel F J, Ortega J E, Mankey G J and Willis R F 1998 Magnetic nanostructures *Adv. Phys.* **47** 511–97 and references therein
[15] Shen J and Kirschner J 2002 Tailoring magnetism in artificially structured materials: the new frontier *Surf. Sci.* **500** 300–22 and references therein
[16] Kodama R H 1999 Magnetic nanoparticles *J. Magn. Magn. Mater.* **200** 359–72 and references therein
[17] Caneschi A, Gatteschi D, Sessoli R and Rey P 1989 Toward molecular magnets-the metal-radical approach *Acc. Chem. Res.* **22** 392–8
[18] Barbara B, Thomas L, Lionti F, Chiorescu I and Sulpice A 1999 *J. Magn. Magn. Mater.* **200** 167–81
[19] Stiles M D 1999 Interlayer exchange coupling *J. Magn. Magn. Mater.* **200** 322–37
[20] Tsymbal E Y and Pettifor D G 2001 Perspectives of giant magnetoresistance *Solid State Phys.* **56** 113–237
[21] Levy P M and S Zhang S 1999 Spin dependent tunnelling *Curr. Opin. Solid State Mater. Sci.* **4** 223
[22] Nogues J and Schuller I K 1999 Exchange bias *J. Magn. Magn. Mater.* **192** 203–32
[23] Schulthess T C and Butler W H 1999 Coupling mechanisms in exchange biased films (invited) *J. Appl. Phys.* **85** 5510–15
[24] Kiwi M 2001 Exchange bias theory *J. Magn. Magn. Mater.* **234** 584–95
[25] Imada M, Fujimori A and Tokura Y 1998 Metal–insulator transitions *Rev. Mod. Phys.* **70** 1039–263
[26] Ohno H 1999 Properties of ferromagnetic III–V semiconductors *J. Magn. Magn. Mater.* **200** 110–29
[27] Awschalom D D and Samarth N 1999 Spin dynamics and quantum transport in magnetic semiconducting quantum structures *J. Magn. Magn. Mater.* **200** 130–47
[28] Moriarty P 2001 Nanostructured materials *Rep. Prog. Phys.* **64** 297–381
Wolf S A, Awschalom D D, Buhrman R A, Daughton J M, von Molnár S, Roukes M L, Chtchelkanova A Y and Treger D M 2001 Spintronics: a spin-based electronics vision for the future *Science* **294** 1488–95
[29] Shchukin V A and Bimberg D 1999 Spontaneous ordering of nanostructures on crystal surfaces **71** 1125–71 and references therein
[30] Moruzzi V L, Markus P M and Kubler J 1989 Magnetovolume instabilities and ferromagnetism versus antiferromagnetism in bulk fcc iron and manganese *Phys. Rev.* B **39** 6957–61
[31] Thomassen J, May F, Feldmann B, Wuttig M and Ibach H 1992 Magnetic live surface layers in Fe/Cu(100) *Phys. Rev. Lett.* **69** 3831–4
[32] Li D Q, Freitag M, Pearson J, Qiu Z Q and Bader S D 1994 Magnetic phases of ultrathin Fe grown on Cu(100) as epitaxial wedges *Phys. Rev. Lett.* **72** 3112–15
[33] Muller S, Bayer P, Reischl C, Heinz K, Feldmann B, Zillgen H and Wuttig M Structural instability of ferromagnetic fcc films on Cu(100) *Phys. Rev. Lett.* **74** 765–8
[34] Biedermann A, Tscheliessnig R, Schmid M and Varga P 2001 Crystallographic structure of ultrathin Fe films on Cu(100) *Phys. Rev. Lett.* **87** 086103
[35] Meinel K, Klaua M and Bethge H 1988 On twin and stacking-fault formation during the expitaxial film growth of fcc materials on (111) substrates *Phys. Status Solidi* a **110** 189–96
[36] Camarero J, de la Figuera J, de Miguel J J, Miranda R, Alvarez J and Ferrer S 2000 Structural characterization and homoepitaxial growth on Cu(111) *Surf. Sci.* **459** 191–205
[37] Tian D, Jona F and Marcus P M 1992 Structure of ultrathin films of Fe on Cu(111) and Cu(110) *Phys. Rev.* B **45** 11216–21

[38] Kim Y, Maeng J Y, Lee S Y and Kim S 2001 Growth properties of ultrathin Fe overlayers grown on a highly stepped Cu(111) surface *Appl. Surf. Sci.* **174** 316
[39] Kief M T and Egelhoff W F 1993 Growth and structure of Fe and Co thin-films on Cu(111), Cu(100), and Cu(110)—a comprehensive study of metastable film growth *Phys. Rev.* B **47** 10785–814
[40] Klaua M, Hoche H and Jenniches H 1997 Strain-driven formation of two-dimensional holes on Cu(111) after the deposition of Fe *Surf. Sci.* **381** 106–16
[41] Ellerbrock R D, Fuest A, Schatz A, Keune W and Bland R A 1995 Mossbauer-effect study of magnetism and structure of fcc-like Fe(001) films on Cu(111) *Phys. Rev. Lett.* **74** 3053–6
[42] Kummerle W and Gradmann U 1978 Magnetic properties of ferromagnetic gamma-Fe films on Cu(111) *Phys. Status Solidi* a **45** 171–80
[43] Rau C, Schneider C, Xing G and Jamison K 1986 Ferromagnetic order at surfaces of ultrathin epitaxial fcc gamma-Fe(111)p(1×1) films on Cu(111) *Phys. Rev. Lett.* **57** 3221–4
[44] Shen J, Klaua M, Ohresser P, Jenniches H, Barthel J, Mohan C V and Kirschner J 1997 Structure and magnetic phase transitions of Fe on stepped Cu(111) *Phys. Rev.* B **56** 11134–43
[45] Castrucci P, Gunnella R, Bernardini R, De Crescenzi M, Ferrari L, Crotti C, Comiccioli C, Ottaviani C, Gubbioti G and Carlotti G 2001 Electronic states and magnetism of ultrathin Fe/Cu/Si(111) films *Surf. Sci.* **476** 43–53
[46] Dong Y H, Qian H J, Ren W W, Krash I, Liu F Q, Meng G, Lin Z D and Wu S C 1998 Observation of an interface state in fcc Fe epitaxially grown on Cu(111) *Solid State Commun.* **108** 111–15
[47] Brodde A, Dreps K, Binder J, Lunau C and Neddermeyer H 1993 Scanning tunnelling microscopy and photoemission from Fe/Cu(111) *Phys. Rev.* B **47** 6609–16
[48] Ohresser P, Ghiringhelli G, Tjernberg O and Brookes N B 2000 Magnetism of nanostructures studied by x-ray magnetic circular dichroism: Fe on Cu(111) *Phys. Rev.* B **62** 5803–9
[49] See e.g.
Chrisey D B and Huebler G K (ed) 1994 *Pulsed Laser Deposition of Thin Films* (New York: Wiley)
[50] Stoyanov S and Kashchiev D 1981 *Current Topics in Materials Science* vol 7, ed E Kaldis (Amsterdam: North-Holland) pp 69–141
[51] Venables J A 1973 Rate equation approaches to thin-film nucleation kinetics *Phil. Mag.* **27** 697–738
Venables J A, Spiller G D T and Hanbuecken M 1984 Nucleation and growth of thin films *Rep. Prog. Phys.* **47** 399–459
[52] Qian D, Jin X F, Barthel J, Klaua M and Kirschner J 2001 Spin-density wave in ultrathin Fe films on Cu(100) *Phys. Rev. Lett.* **87** 227204
[53] Ohresser P, Shen J, Barthel J, Zheng M, Mohan C V, Klaua M and Kirschner J 1999 Growth, structure, and magnetism of fcc Fe ultrathin films on Cu(111) by pulsed laser deposition *Phys. Rev.* B **59** 3696–706
[54] Hobbs D and Hafner J 2000 Fully unconstrained non-collinear magnetism in triangular Cr and Mn monolayers and overlayers on Cu(111) substrates *J. Phys.: Condens. Matter* **12** 7025–40
[55] Ujfulussy B 2002 private communication
[56] Zharnikov M, Dittschar A, Kuch W, Schneider C M and Kirschner J 1996 Magnetic order–disorder transition mediated by a temperature-driven structural transformation *Phys. Rev. Lett.* **76** 4620–3
[57] Landau L D and Lifshitz E M *Statistical Physics, Theoretical Physics* vol 5 (Moscow: Nauka)
The theorem on the last page of their book basically states that at any non-zero temperature, the free energy gained from the entropy due to breaking a chain exceeds the free energy loss from the energy associated with the break
[58] Callaway J *Quantum Theory of the Solid State* (New York: Academic)
(see section 7.5) The resistance of a one-dimensional disordered chain is predicted to increase exponentially with its length
[59] Haldane F D M 1983 Non-linear field-theory of large-spin Heisenberg anti-ferromagnets—semi-classically quantized solitons of the one-dimensional easy-axis Néel state *Phys. Rev. Lett.* **50** 1153–6
[60] Shen J, Skomski R, Klaua M, Jenniches H, Manoharan S S and Kirschner J 1997 Magnetism in one dimension: Fe on Cu(111) *Phys. Rev.* B **56** 2340–3
[61] Li D Q, Cuenya B R, Pearson J, Bader S D and Keune W 2001 Magnetism of step-decorated Fe on Pd(110) *Phys. Rev.* B **64** 144410
[62] Kubetzka A, Bode M, Pietzsch O and Wiesendanger R 2002 Spin-polarized scanning tunnelling microscopy with antiferromagnetic probe tips *Phys. Rev. Lett.* **88** 057201
[63] Pierce J P, Shen J and Plummer E W 2002 Ferromagnetism in cobalt-iron alloy nanowire arrays on W(110) *Appl. Phys. Lett.* **81** 1890
[64] Shen J, Giergiel J, Schmid A K and Kirschner J 1995 Surface alloying and pinhole formation in ultra-thin Fe/Cu(100) films *Surf. Sci.* **328** 32–46

[65] Gai Z, Pierce J P, Farnan G A and Shen J 2002 Growth of low-dimensional magnetic nanostructures on an insulator *Appl. Phys. Lett.* **81** 742
[66] Tober E D, Farrow R F C, Marks R F, Witte G, Kalki K and Chambliss D D 1998 Self-assembled lateral multilayers from thin film alloys of immiscible metals *Phys. Rev. Lett.* **81** 1897–900
[67] Sugawara A, Coyle T, Hembree G G and Scheinfein M R 1997 Self-organized Fe nanowire arrays prepared by shadow deposition on NaCl(110) templates *Appl. Phys. Lett.* **70** 1043–5
[68] Fert A and Piraux L 1999 Magnetic nanowires *J. Magn. Magn. Mater.* **200** 338–58
[69] Zhang Z, Dai S, Blom D A and Shen J 2002 Synthesis of ordered metallic nanowires inside ordered mesoporous materials through electroless deposition *Chem. Mater.* **14** 965
[70] Hauschild J, Elmers H J and Gradmann U 1998 Dipolar superferromagnetism in monolayer nanostripes of Fe(110) on vicinal W(110) surfaces *Phys. Rev.* B **57** R677–80
[71] Shen J, Skomski R, Klaua M, Jenniches H, Manoharan S S and Kirschner J 1997 Magnetism in one dimension: Fe on Cu(111) *Phys. Rev.* B **56** 2340–3
[72] Yeomans J M 1992 *Statistical Mechanics of Phase Transitions* (Oxford: Oxford University Press)
[73] Brown G, Lee H K, Schulthess T C, Ujfalussy B, Stocks G M, Butler W H, Landau D P, Pierce J P, Shen J and Kirschner J 2002 Model of Fe nanostripes on Cu(111) *J. Appl. Phys.* **91** 7056–8
[74] Huang L, Chey S J and Weaver J H 1998 Buffer-layer-assisted growth of nanocrystals: Ag–Xe–Si(111) *Phys. Rev. Lett.* **80** 4095–8
[75] Chey S J, Huang L and Weaver J H 1998 Self-assembly of multilayer arrays from Ag nanosclusters delivered to Ag(111) by soft landing *Surf. Sci.* **419** L100–6
[76] Pierce J P, Gai Z, Farnan G A, Wendelken J F, Plummer E W and Shen J 2002 Magnetism in buffer-layer grown Fe nanodots on Cu(111) to be submitted
[77] Zhang Z Y and Wendelken J F 2001 B1: Self organized formation of a material on a substrate *US Patent Specification* 6,313,479
[78] Lee H K, Schulthess T C, Landau D P, Brown G, Pierce J P, Gai Z, Farnan G A and Shen J 2002 Monte Carlo simulations of interacting magnetic nanoparticles *J. Appl. Phys.* **91** 6926–8
[79] Bruno P 1988 *J. Phys. F: Met. Phys.* **18** 1291–8